THE JOURNAL OF PHYSICAL CHEMISTRY C

Article

Cite This: J. Phys. Chem. C XXXX, XXX, XXX−XXX

pubs.acs.org/JPCC

Internalization of a Preformed Atomically Precise Silver Cluster in Proteins by Multistep Events and Emergence of Luminescent Counterparts Retaining Bioactivity

Debasmita Ghosh,[†] Mohammad Bodiuzzaman,[†] Anirban Som,[†] Sebastian Raja,[‡] Ananya Baksi,[†] Atanu Ghosh,[†] Jyotirmoy Ghosh,[†] Akshayaa Ganesh,[‡] Priyanka Samji,[‡] Sundarasamy Mahalingam,[‡] Devarajan Karunagaran,[‡] and Thalappil Pradeep*[,†]

[†]DST Unit of Nanoscience (DST UNS) and Thematic Unit of Excellence, Department of Chemistry and [‡]Department of Biotechnology, Indian Institute of Technology Madras, Chennai 600036, India

Supporting Information

ABSTRACT: A new synthetic protocol is introduced which preserves the secondary structure of protecting proteins encapsulating a luminescent atomically-precise silver cluster. This was achieved by using a preformed triphenylphosphine (TPP)-protected silver cluster as the precursor forming bovine serum albumin (BSA)- and human serum albumin (HSA)-protected Ag_{18} clusters. This is the first example of the formation of luminescent protein-protected clusters in a neutral medium, without using any reducing agent, which results in minimal alteration of the protein structure during cluster growth. The cluster formed showed exceptional stability, unlike other silver clusters of this class. The formation of these red luminescent clusters was visualized by UV−vis and photoluminescence spectroscopy. The identification of Ag_{18} core was made through matrix-assisted laser desorption ionization mass spectrometry (MALDI MS), and a plausible mechanism of the formation was identified by monitoring the systematic growth of the cluster core by time-dependent MALDI MS experiments and electrospray ionization mass spectrometry (ESI MS) of the reaction mixture. The cluster was successfully employed as a luminescent probe for cancer cell imaging. Retention of protein conformation in the clusters was confirmed through circular dichroism (CD) spectroscopy, and the same was reflected in the retention of 89% of the esterase activity of BSA in the Ag_{18}@BSA clusters synthesized by this method, compared to only 28.7% for Ag_{QC}@BSA clusters synthesized using previous protocols, conducted in basic medium.

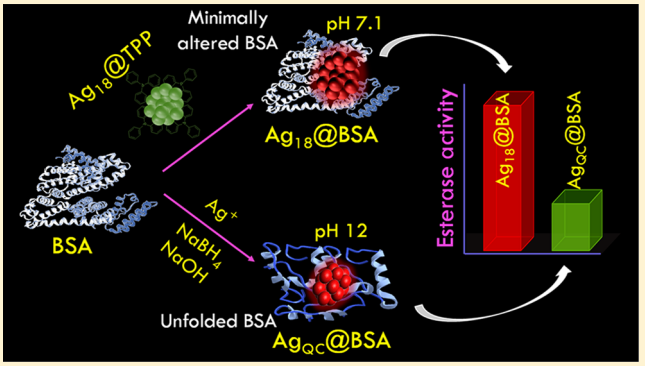

INTRODUCTION

Protein-protected noble metal nanoclusters (NCs),[1−3] a subclass of atomically-precise protected noble metal clusters,[4,5] are the most studied ones among this class of materials. Due to their intense luminescence with high quantum yield, stability in ambient condition for months, and biocompatibility, these materials are considered as a new class of biohybrid materials with potential applications in diverse areas,[6,7] especially in sensing[8−10] and biology.[11−14] Development of such stable, sensitive, and reliable platforms are highly desirable for specific binding and targeted drug delivery,[15,16] multimodal imaging,[17−19] therapeutic applications,[20] targeted biolabeling,[2,21,22] and so on. Bovine serum albumin (BSA) is the most commonly used protein to synthesize Au and Ag clusters like Au_9@BSA,[23] Au_{16}@BSA,[24] Au_{25}@BSA,[1] Au_{30}@BSA,[25] Au_{38}@BSA,[21] Ag_8@BSA,[26] Ag_{15}@BSA,[27] and Ag_{31}@BSA.[28] Other than BSA, large proteins with high molecular weight such as human serum albumin (HSA) (Au@HSA),[29] lactotransferrin ($Au_{25,34,40}$),[30,31] human serum transferrin (Au),[32] pepsin ($Au_{8,13,25}$),[33] horseradish peroxidase (Au),[34] egg white (Au, Pt),[35] and ovalalbumin (Au)[36] have been employed to synthesize Au, Pt, and Ag clusters. Small proteins with low molecular weight such as insulin (Au),[37] lysozyme ($Au_{8,10-12}$),[10,38] and trypsin (Au)[39] have also been used to synthesize protein-protected clusters. In all of these cases, gold is preferred to make such clusters due to the ease of synthesis and greater stability of the resultant clusters, and the number of silver clusters reported is substantially less.

In a typical protein-directed cluster synthesis, the metal ion is complexed with the protein and subsequently reduced either by a strong reducing agent, like $NaBH_4$, or by increasing the pH (11−12) of the solution.[1,27,28] However, in the presence of a strong reducing agent ($NaBH_4$) or alkaline pH of the reaction mixture, proteins undergo irreversible conformational changes, and this results in the partial or complete loss of their inherent bioactivity.[40,41] Sometimes it leads to the formation of

Received: August 14, 2019
Revised: November 4, 2019
Published: November 11, 2019

DOI: 10.1021/acs.jpcc.9b07765
J. Phys. Chem. C XXXX, XXX, XXX−XXX

protein oligomerization.[42,43] Reduced bioactivity is one of the factors limiting the widespread use of such materials in biomedical research. Therefore, a milder synthetic method retaining the bioactivity of the as-synthesized NCs is needed. With these objectives, we explored the possibility of using preformed clusters as precursors to synthesize luminescent clusters, retaining the bioactivity of the protein.

Phosphine-protected clusters of gold have been known and studied for some time.[4,44] A new class of atomically precise NCs of silver coprotected by hydride and phosphines as ligands was reported recently.[45,46] Such clusters are expected to be more reactive, having accessible metal sites compared to the thiol-protected clusters due to the presence of labile phosphines. Here we report that such a cluster, $[Ag_{18}H_{16}(TPP)_{10}]^{2+}$ (to be abbreviated as I subsequently), where TPP is triphenylphosphine, can be systematically transformed into highly stable and luminescent silver clusters protected by proteins under neutral pH conditions, preserving the bioactivity of the encapsulating proteins. The precursor I acts as a source of atomic Ag species toward the formation of the red luminescent Ag_{18}@BSA at neutral pH. The retention of the protein's bioactivity and secondary structure in the course of cluster formation has been confirmed experimentally. Such transformations were not observed with more stable nanoparticles and thiol-protected cluster systems, implying the sensitivity of the method to the specificity and chemical stability of the starting materials.

METHODS

Materials. $AgNO_3$ was purchased from Rankem Chemicals. Sodium borohydride ($NaBH_4$, 98%) was purchased from Sigma-Aldrich. Triphenylphosphine (TPP) was purchased from Spectrochem. BSA was purchased from the Sisco Research Laboratory. All of the chemicals were used as received without further purification. All solvents (dichloromethane (DCM), methanol (MeOH)) were purchased from Rankem and were of analytical grade. Milli-Q water with a resistivity of 18.2 MΩ·cm was used for synthesis. The protein, BSA, contained Na^+ in the as-received form.

Instrumentation. UV−vis spectra were recorded using a PerkinElmer Lambda 25 UV−vis spectrometer. Absorption spectra were typically measured in the range of 200−1100 nm with a band-pass filter of 1 nm.

MALDI MS of Ag_{18}@BSA cluster was measured using a Voyager-DE PRO Biospectrometry Workstation from Applied Biosystems. A pulsed nitrogen laser of 337 nm was used for ionizing the sample, and sinapic acid was used as the matrix. Spectra were collected in the positive mode, and an average of 250 shots was used for each spectrum. The matrix solution was prepared by dissolving 10 mg of sinapic acid in a 1:3 mixture of acetonitrile and 0.1% trifluoroacetic acid (TFA) in Milli-Q water (overall volume of 1 mL). A 5 μL amount of the cluster solution, without dilution, was mixed thoroughly with 50 μL of the matrix mixture. A 2.5 μL amount of the resulting mixture was used for spotted by dried droplet method.

ESI MS experiments were done using a Waters Synapt G2Si HDMS instrument. The instrument consists of an electrospray source, quadrupole ion guide/trap, ion mobility cell, and TOF detector. All of the experiments were done in positive ion mode.

Photoluminescence measurement was carried out in a HORIBA, Jobin Yvon NanoLog Fluorescence spectrometer with a band pass of 3 nm for both emission and excitation spectra.

Circular dichroism (CD) spectra were measured in a Jasco 815 spectropolarimeter with Peltier setup for the temperature-dependent measurements. CD studies were done with a 10 mm path length cell. The concentration of the sample in the cuvette used for CD measurement was 2×10^{-7} g mL^{-1}.

Scanning electron microscopy (SEM) and energy-dispersive analysis (EDS) images were conducted using an FEI QUANTA-200 SEM. For the measurements (SEM and EDS), samples were spotted on an indium tin oxide (ITO) conducting glass substrate and dried in ambient conditions.

High-resolution transmission electron microscopy (HRTEM) was performed with a JEOL 3010, 300 kV instrument equipped with an ultrahigh-resolution (UHR) pole piece. Samples were prepared by dropping the dispersion on carbon-coated copper grids for HRTEM.

The cells were imaged using a LSM880 laser scanning confocal microscope (Carl Zeiss, Germany), and image acquisition was performed using a high-NA oil immersion objective (Plan-Apochromat 63×/1.4) using Zen 2009 software (Carl Zeiss, Germany). Laser lines at 405 and 488 nm were used for excitation. For 405 nm excitation, emission was collected from 410 to 550 nm, and for 488 nm excitation, emission was collected from 491 to 550 nm. Each image was acquired with an exposure time of 80 and 100 ms. The total thickness of the sample was about 4−5 μm, leading to the acquisition of 25−30 optical sections. Images were processed through Zen BLACK software (Carl Zeiss) and exported into TIF format. Selected cellular regions were cropped and analyzed further in ZEN Blue software for 3D reconstruction with a 180-frame rotation series along the *Y* axis. The orthogonal view and 3-D images reconstruction were made using ZEN Blue software. The intracellular distribution was projected using Imaris 3D rendering software.

Synthesis of $[Ag_{18}H_{16}(TPP)_{10}]^{2+}$ (Cluster I). Initially, 20 mg of $AgNO_3$ was dissolved in 5 mL of methanol. To the above solution TPP (70 mg in 10 mL of chloroform) was added under stirring conditions. After 20 min, 6 mg of $NaBH_4$ dissolved in 0.5 mL of ice-cold Milli-Q water was added to the above reaction mixture. After addition of aqueous $NaBH_4$ solution, the colorless solution immediately turned light yellow. The stirring was continued for 3 h. The final color of the solution was deep green, which confirmed the formation of cluster. The solvent was removed from the reaction mixture by rotary evaporation. The cluster was then washed 6−7 times with Milli-Q water to remove the unreacted silver ions and $NaBH_4$. After being washed, the green-colored precipitate was dissolved in 1 mL of methanol. The final concentration of I is 15 mM.

Synthesis of $[Ag_{18}$@BSA]. A 25 mg amount BSA was dissolved in 1.6 mL of Milli-Q water. Then the solution was stirred for 1 min. Under stirring condition 400 μL of I was added from the 1 mL of methanol solution. The addition of I into the BSA solution made the reaction mixture turbid. Stirring was continued for 12 h. The turbid solution was centrifuged, and from the supernatant the brown-colored cluster solution was collected. This solution was used for characterization.

Synthesis of $[Ag_{QC}$@BSA]. A 5 mL amount of 10 mM silver nitrate solution was added to a solution of 250 mg of BSA dissolved in 5 mL of Milli Q water with vigorous stirring at room temperature. About 0.3 mL of 1 M NaOH solution

DOI: 10.1021/acs.jpcc.9b07765
J. Phys. Chem. C XXXX, XXX, XXX−XXX

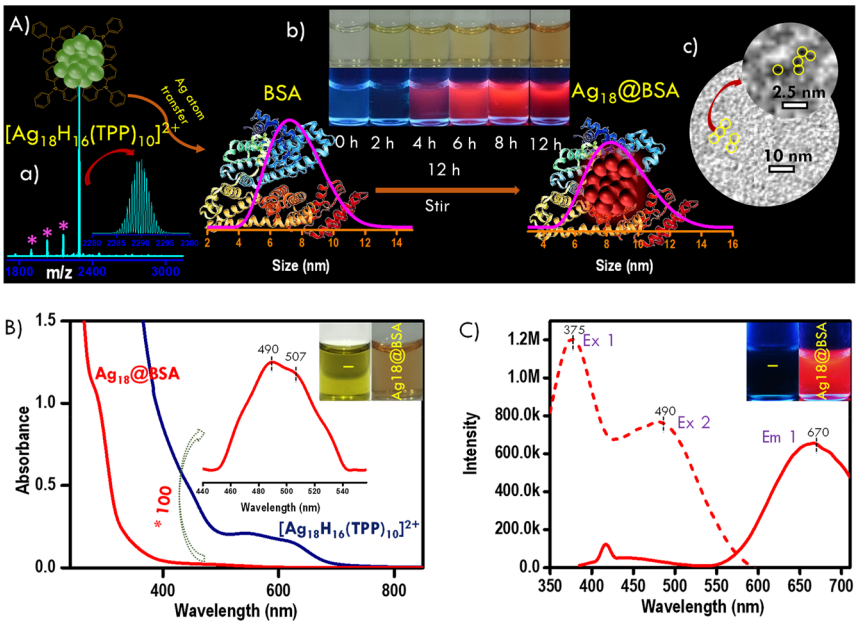

Figure 1. (A) Schematic of the formation of Ag_{18}@BSA from I. Hydrodynamic diameters of BSA and Ag_{18}@BSA are shown in the schematic. ESI MS of I is shown in inset a, where peaks marked with asterisks (*) are due to the phosphine losses from I. Expanded view of the molecular ion peak is also shown. Pictorial representation of the time-dependent change in color of the solution under visible and UV light is shown as inset b. TEM image of Ag_{18}@BSA is shown as inset c. Cluster cores are marked. (B) UV−vis spectra of Ag_{18}@BSA and I. Inset shows the solutions of I and Ag_{18}@BSA under visible light. (C) Luminescence profile of Ag_{18}@BSA. Inset shows the solutions of I and Ag_{18}@BSA under UV light. Absorption and emission maxima are marked on the traces. Concentration of Ag_{18}@BSA cluster solution is 7.5×10^{-4} mol/L.

was added followed by 10 mM $NaBH_4$ solution dropwise until the solution turns from colorless to reddish brown, indicating formation of the Ag_{QC}@BSA cluster.

Cell Viability. The cellular toxicity of Ag_{18}@BSA was determined by resazurin reduction, a colorimetric assay. HeLa cells were seeded in a 96-well plate at a density of 5000 per well and grown overnight. They were treated with different concentrations of the clusters. After 24 h of incubation, each well was washed with phosphate-buffered saline. Resazurin dye was added and incubated for the 3 h for the reduction. The blue dye resazurin became to pink resorufin, and the absorbance was measured at 570 and 595 nm. Three replicates were performed.

Cellular Uptake Studies by Confocal Fluorescence Microscopy. HeLa cells were cultured on chamber slides (BD Biosciences, USA) and incubated with Ag_{18}@BSA (5 μM concentration) NCs for 5 and 24 h. After incubation, the cells were fixed with 4% (w/v) paraformaldehyde followed by permeabilization using 0.1% Triton X-100 and washed with PBS buffer. The cells were mounted in the mounting medium (Vector Laboratories, USA) containing Hoechst 33342 to stain the nuclei. These cells were covered with a coverslip, sealed with nail polish, and kept for imaging.

Evaluation of Esterase Activity. The bioactivity of BSA and the Ag_{18}@BSA was determined by monitoring the appearance of the hydrolysis product of *p*-nitro-phenyl acetate (PNA) in a manner similar to a previously reported method.[47] The concentration of PNA was 100 μM, and the concentrations of BSA and Ag_{18}@BSA were 1 mg/mL.

RESULTS AND DISCUSSION

Luminescent Cluster from a Nonluminescent one. Synthesis of Ag_{18}@BSA was initiated by mixing I with a solution of BSA at pH 7.1 under continuous magnetic stirring.

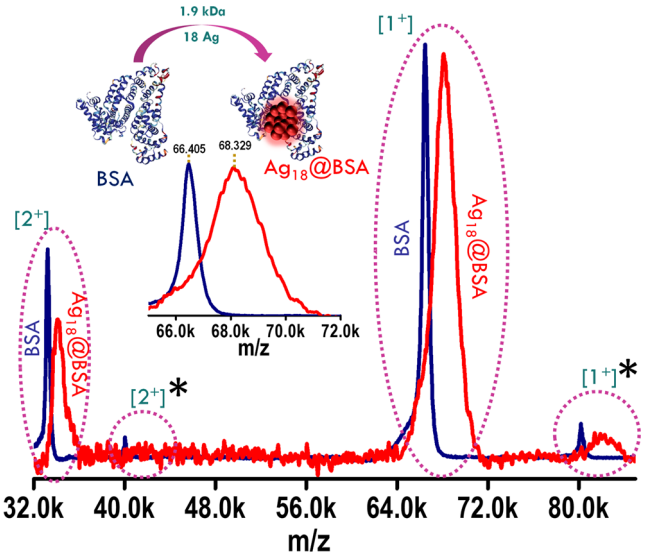

Figure 2. MALDI MS of pure BSA (blue trace) collected in the linear positive ion mode using sinapic acid as the matrix and that of as-prepared, red-emitting Ag_{18}@BSA (red trace). Peaks due to singly charged ions of Ag_{18}@BSA are expanded in the inset along with those of BSA. Presence of conalbumin in the BSA is indicated with an asterisk (*).

A schematic of the formation of Ag_{18}@BSA from I (ESI MS shown in inset a) is represented in Figure 1A. A gradual color change of the mixture during the course of the reaction was observed, accompanied by the evolution of red luminescence, generally associated with the formation of metal clusters. The time evolution of cluster growth observed under visible and UV illumination is shown in the inset b of Figure 1A. Such a gradual change in color and luminescence of the protein

DOI: 10.1021/acs.jpcc.9b07765
J. Phys. Chem. C XXXX, XXX, XXX−XXX

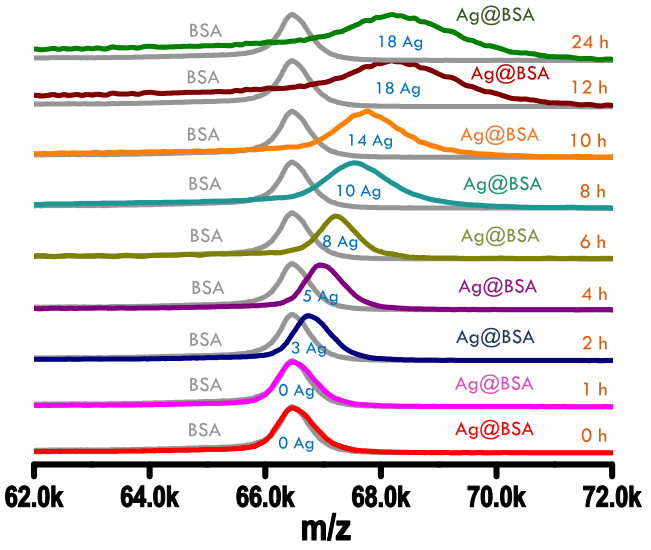

Figure 3. Time-dependent MALDI MS showing the evolution of Ag_{18}@BSA cluster. MALDI MS of parent BSA is shown for comparison.

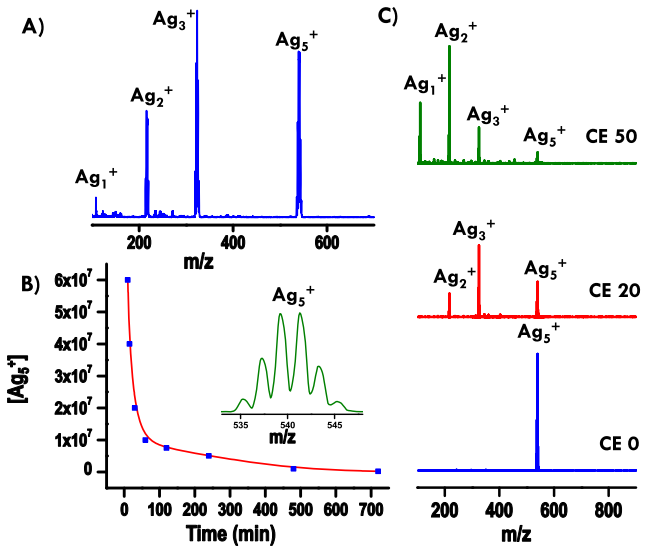

Figure 4. (A) ESI MS of the reaction mixture after 10 min, showing the presence of small Ag clusters. (B) Decay in the ion intensity of Ag_5^+ with the progress of the reaction. Isotopic distribution of Ag_5^+ is shown in the inset. (C) MS/MS study of Ag_5^+, showing the formation of other small Ag clusters can arise from the fragmentation of Ag_5^+. Collision energy (CE) is in instrumental limit.

solution indicated slow nucleation of the cluster core within the protein template. After 12 h of reaction, a colorless BSA solution turned into a brown-colored, intense red luminescent solution. No perceptible change in the color of the solution was observed when incubation was continued beyond 12 h. Monolayer-protected NCs generally exhibit well-defined molecular transitions in the absorption profile.[4] The blue trace in Figure 1B shows the UV−vis spectrum of precursor I with maxima at 550 and 620 nm.[45,46] The UV−vis spectrum of Ag_{18}@BSA (red trace, Figure 1B) predominantly exhibits the characteristic absorption of BSA at 280 nm along with a broad absorption in the 440−540 nm region. Expansion of this region (inset of the Figure 1B) clearly shows two absorption maxima around 490 and 507 nm, further indicating the formation of a protein-protected silver cluster. The change in the color of the cluster solution from green (parent I) to brown (formed Ag_{18}@BSA NCs) under visible light is shown in the inset of Figure 1B. The photoluminescence profile of the cluster (Figure 1C) shows two excitation peaks around 375 and 490 nm along with a bright red emission centered around 670 nm. The excitation maximum at 375 nm is due to the presence of the protein shell, and the other excitation maximum at 490 nm is because of the presence of the cluster core. Both excitations give the same emission but with different intensities. Photographs under UV illumination showing the transformation of I into a red luminescent cluster are presented in the inset of Figure 1C. The quantum yield of the cluster was 25.1% using fluorescein as reference (in water). It is also worth mentioning that in the course of formation of the protein-protected NCs in solution an insoluble product was also formed, which was removed through centrifugal precipitation, and the centrifugate containing the NCs was characterized in detail. EDS analysis of the precipitate formed after 12 h showed the presence of water-insoluble phosphines along with Ag and proteins (Figure S1).

Formation of the cluster core in the protein template results in swelling of the protein.[48] The hydrodynamic diameter of the parent BSA was 7.2 nm. At the end of the reaction, the average size of the proteins was increased by about 1 nm, as shown in Figure 1A. It is very difficult to determine the exact core size for clusters from HRTEM analysis as the high-energy electron beam is known to induce cluster coalescence. Low-dose microscopy was performed to confirm the formation as well as to have a definite idea about the size of the cluster core. The cluster core appears as tiny black dots in the HRTEM image (inset c, Figure 1A) having a size of ∼1 nm. This also confirmed the absence of bigger plasmonic nanoparticles in solution.

Identification of the Atomicity. Mass spectrometry has emerged as an essential tool in understanding the atomicity of the clusters. We measured the MALDI MS of the as-prepared NCs to assign the nuclearity of the cluster core. The spectra of the cluster (red trace) and of BSA (blue trace) are shown in Figure 2. BSA showed its molecular ion peak at m/z 66.4 kDa and a peak at m/z 33.2 kDa, corresponding to the +2 charge state in the MS. In the case of the cluster, both peaks were seen, albeit they appear at higher masses from that of BSA. The mass shift to a higher mass region in the NCs from the parent protein in both +1 and +2 states clearly indicate the growth of a cluster core in the protein cavity. An expanded view of the +1 region of the MS (inset, Figure 2) shows a 1.9 kDa shift, corresponding to the incorporation of 18 Ag atoms into the protein core, forming Ag_{18}@BSA. The dication shows one-half the shift, as expected. This confirms that the cluster core is incorporated in a single protein moiety. It is to be noted that the peaks around m/z 80 kDa (+1 charge) and m/z 40 kDa (+2 charge) present in the MALDI MS are associated with the presence of the protein conalbumin, an internal standard used in BSA.[27,49] These peaks were shifted to higher mass in the case of the cluster. This increased shift is attributed to the formation of Ag_{18} core in this protein also.

The EDS spectrum collected from the NCs showed the presence of Ag and S in the formed cluster (Figure S2). Quantitative analysis of the EDS spectrum gives an S:Ag ratio of 2.2, expected for the Ag_{18}@BSA composition (2.22). Note that BSA has 35 S atoms due to cysteine and 5 S atoms due to methionine. XPS spectra in the Ag 3d region (Figure S3)

DOI: 10.1021/acs.jpcc.9b07765
J. Phys. Chem. C XXXX, XXX, XXX−XXX

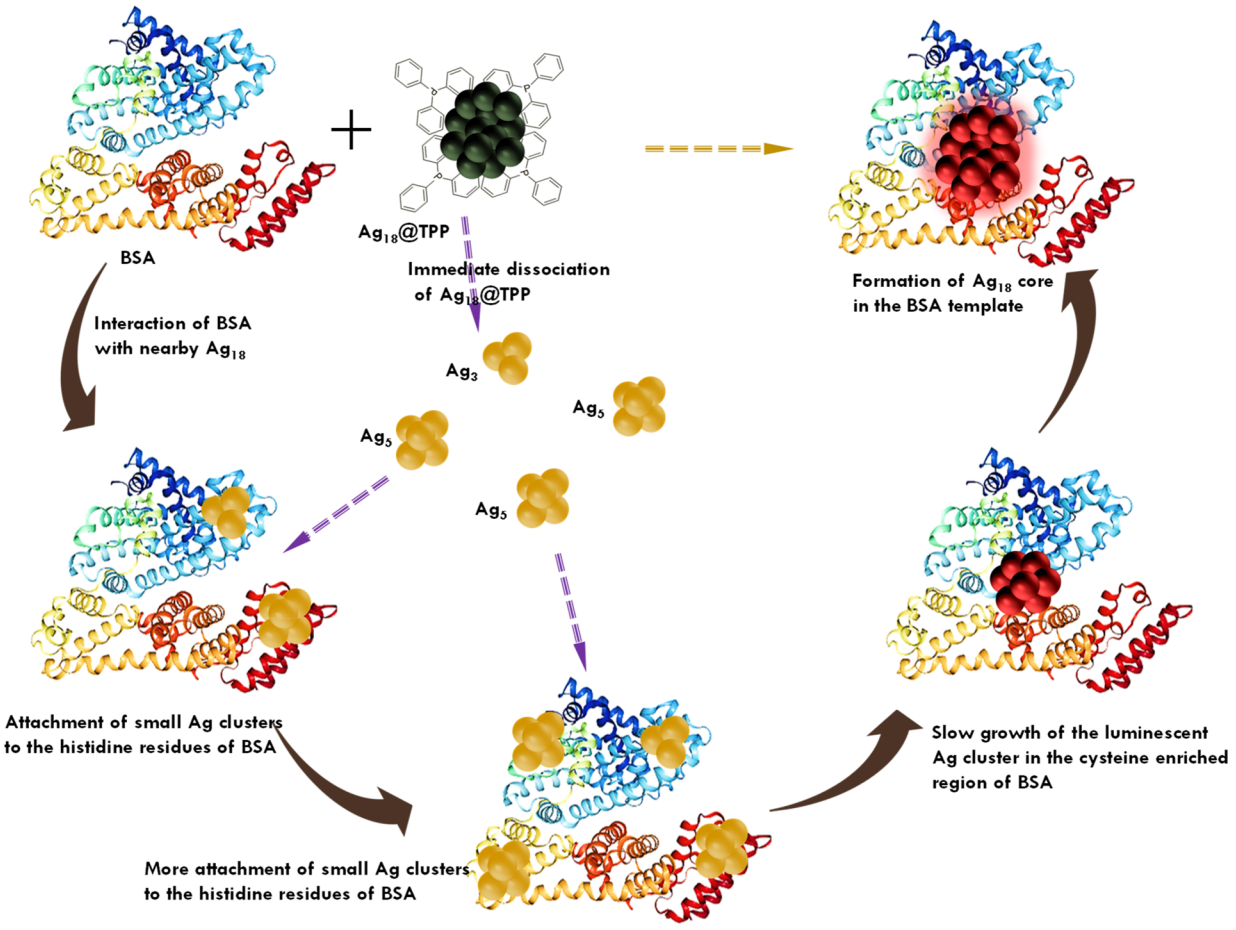

Figure 5. Probable mechanism of the formation of Ag_{18}@BSA from I.

shows Ag in zero (0) oxidation state (Ag $3d_{5/2}$ at 368 eV), and the S 2p region shows S to be thiolate kind (S $2p_{3/2}$ at 161.5 eV) in Ag_{18}@BSA NCs.[27] It further confirmed the chemical composition of the cluster.

Cysteine as well as methionine residues in the proteins are perceived to be responsible for protecting the metal core through the formation of metal−sulfur (M−S) bonds in the protein-protected NCs.[38,50,51] Nuclearity of the cluster cores formed in the proteins, for this reason, depends on the number of cysteine residues present in a particular protein. We chose human serum albumin (HSA), a protein with the same number of cysteine residues as that of BSA to form the cluster through the addition of I. This was also seen to uptake Ag atoms from the precursor cluster, forming Ag_{18}@HSA after 12 h. The UV−vis spectra, luminescence profile, and MALDI MS corresponding to this transformation are shown in Figures S4 and S5.

Lactoferrin (Lf), an 83 kDa protein with different number and position of cysteine and methionine groups, was also used to synthesize Ag NCs following our new method. UV−vis and luminescence spectra of the new system are shown in Figures S6A and S6B, respectively. The MALDI MS shown in Figure S6C confirmed the formation of Ag_{13}@Lf cluster. The difference in atomicity is attributed to the structural differences, stabilizing a smaller cluster. Though the molecular weight of Lf is higher than BSA and HSA, the number of histidine (His) residues present in Lf is less. Thus, the ability of Lf to stabilize the small clusters formed at the initial stage is expected to be lower than both BSA and HSA. This probably results in the formation of a smaller 13-atom Ag cluster in this case. Relevant data are summarized in Table S1.

Mechanism of Multistep Evolution of the Cluster. Formation of Ag_{18}@BSA through the reaction between I and BSA was accompanied by a gradual change in the luminescence of the solution (inset b, Figure 1A and Figure S7). This indicated a gradual evolution of the Ag_{18} cluster during the course of the reaction. To shed light into the time evolution, time-dependent MALDI MS was recorded from aliquots collected at different intervals, as shown in Figure 3. At the initial stages of the reaction (0−1 h), no mass shift from the parent BSA peak was seen. This indicated a different pathway of cluster formation in the current method than the traditional method, in which attachment of metal ions to the protein at the beginning of the reaction is manifested by an abrupt mass shift just after addition of the metal salt.[31] Such a shift is not noticed here as shown by the 0 and 1 h spectra. With further progression of the reaction, a gradual shift to higher mass was seen in the MS up to 12 h, indicating growth of the cluster core inside the protein template over time. The nuclearity reaches Ag_{18} after 12 h, and neither the continuation of the reaction beyond this point nor further addition of fresh I to the reaction mixture changes the final Ag_{18}@BSA. Once formed, the cluster was stable for months, even when stored at room temperature, an attribute generally seen only in gold clusters.

Time-dependent MALDI MS suggests that the formation of Ag_{18}@BSA from I happens slowly, in steps, rather than through transfer of the Ag core from the monolayer protected cluster

DOI: 10.1021/acs.jpcc.9b07765
J. Phys. Chem. C XXXX, XXX, XXX−XXX

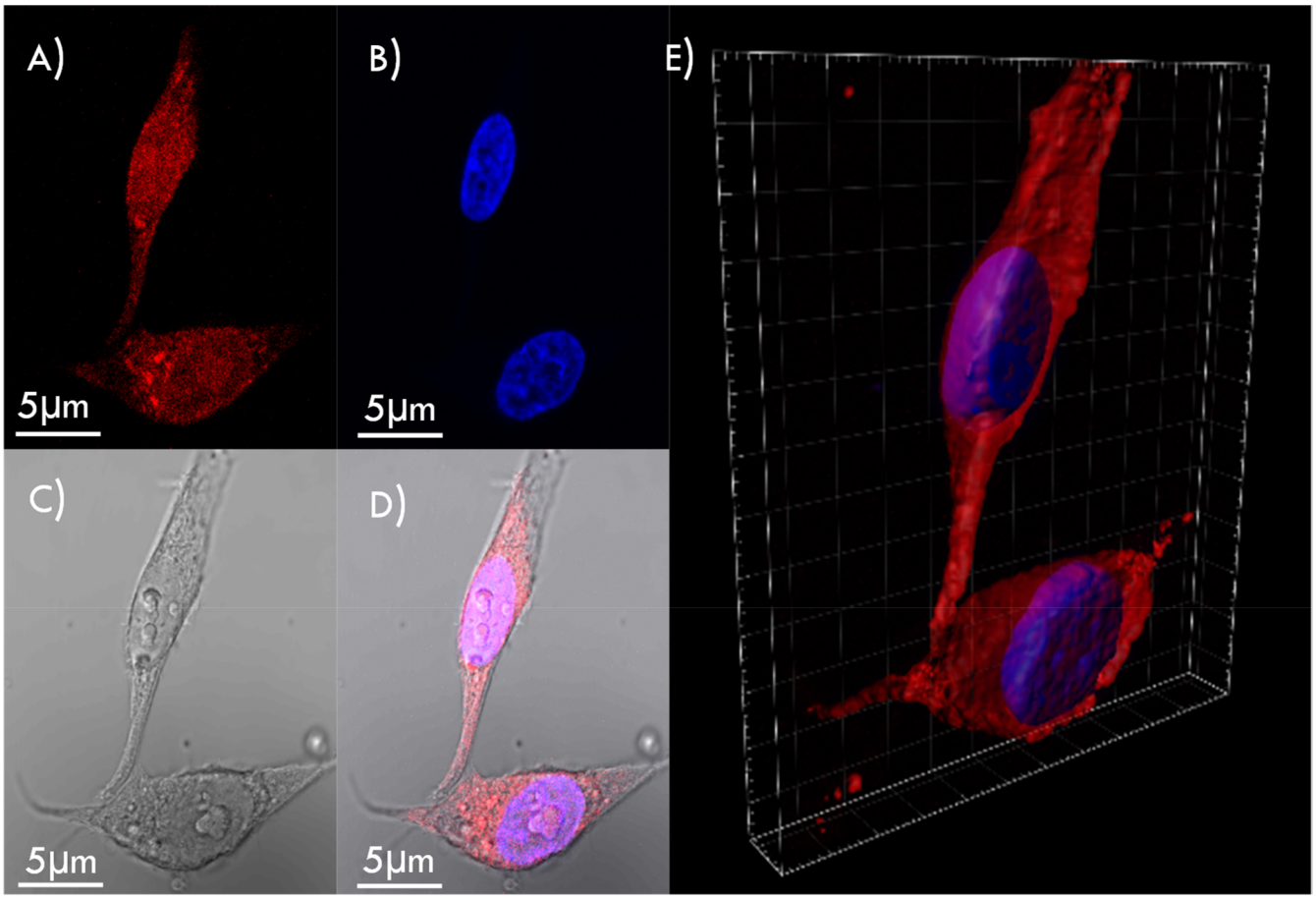

Figure 6. Confocal microscopic images of internalization of Ag_{18}@BSA cluster in HeLa cells after 24 h incubation. (A) Fluorescence image of NCs exhibiting red luminescence inside the cell. (B) Cell nucleus stained with DAPI. (C) Bright-field image of the corresponding cells. (D) Overlay of these three images. (E) 3D reconstruction of the cells confirming internalization of the cluster.

into the protein in a single step. To gain further insight into the mechanism of formation of Ag_{18}@BSA, ESI MS of the reaction mixture was collected at various stages of the reaction. ESI MS of the reaction surprisingly showed the presence of small naked Ag clusters (Figure 4A). The few atom naked Ag clusters were observed at maximum intensities in ESI MS at the early stages of reaction, and their concentration (ion intensity) diminishes as the reaction progresses (Figure 4B). Ag_5^+ appeared as one of the major peaks in the ESI MS, and MS/MS of the same showed that other clusters seen could very well be its fragmentation products (Figure 4C). Ag_4^+ was not seen in ESI MS and is due to lower stability of the three-electron system (Ag_4^+). For this reason Ag_5^+ directly fragmented to Ag_3^+ during MS/MS study. It could also be due to the stability of the neutral fragment, Ag_2. While ESI MS of the reaction mixture at the early stages of the reaction showed the clear presence of naked clusters, MALDI MS at these stages did not indicate formation of any protein-protected cluster species. This led us to infer that the Ag_{18} cluster with labile phosphine protection slowly disintegrates under the reaction conditions, releasing the few atom Ag clusters into the protein molecules present in solution, which immediately captures these small clusters. It is important to note that the proximity of the protein molecules to the released few atom silver clusters play an important role in the stabilization of such clusters. Formation of larger silver nanoparticles was observed when the protein concentration in the reaction mixture was decreased by 1 order of magnitude (Figure S8). The protein molecules remain further apart in solution at this lower concentration, so they cannot capture and protect the small Ag clusters efficiently enough, and they grow into larger nanoparticles.

The initial attachment between the few atom Ag clusters and BSA, however, happens through weak interactions and results in their detachment during mass spectrometric ionization processes (ESI and MALDI). This leads to the observation of naked Ag cluster in ESI MS, while only free protein is observed in the MALDI MS. Stabilization of small Au clusters at the His residues of crystalline protein cage (apoferritin) has been reported recently.[52] We believe that similar attachment of the Ag clusters at the His residues of BSA is responsible for their initial stabilization. These clusters attached to His are then slowly transferred to cysteine (Cys) residues of the protein through the formation of M−S bonds with better thermodynamic stability. This initiates the formation of protein-protected cluster species. The cluster core protected by Cys continues to grow in size with time through the sequential transfer of His-bound Ag cluster followed by their coalescence. These stable cluster species, although unfortunately did not ionize in ESI MS, are seen in MALDI MS as intermediates. Growth of the protein-protected cluster core with time also results in the reduction of the concentration of His-bound Ag cluster. This was reflected in the decrease in the ion intensity of the naked clusters with reaction time (Figure 4B). The

DOI: 10.1021/acs.jpcc.9b07765
J. Phys. Chem. C XXXX, XXX, XXX−XXX

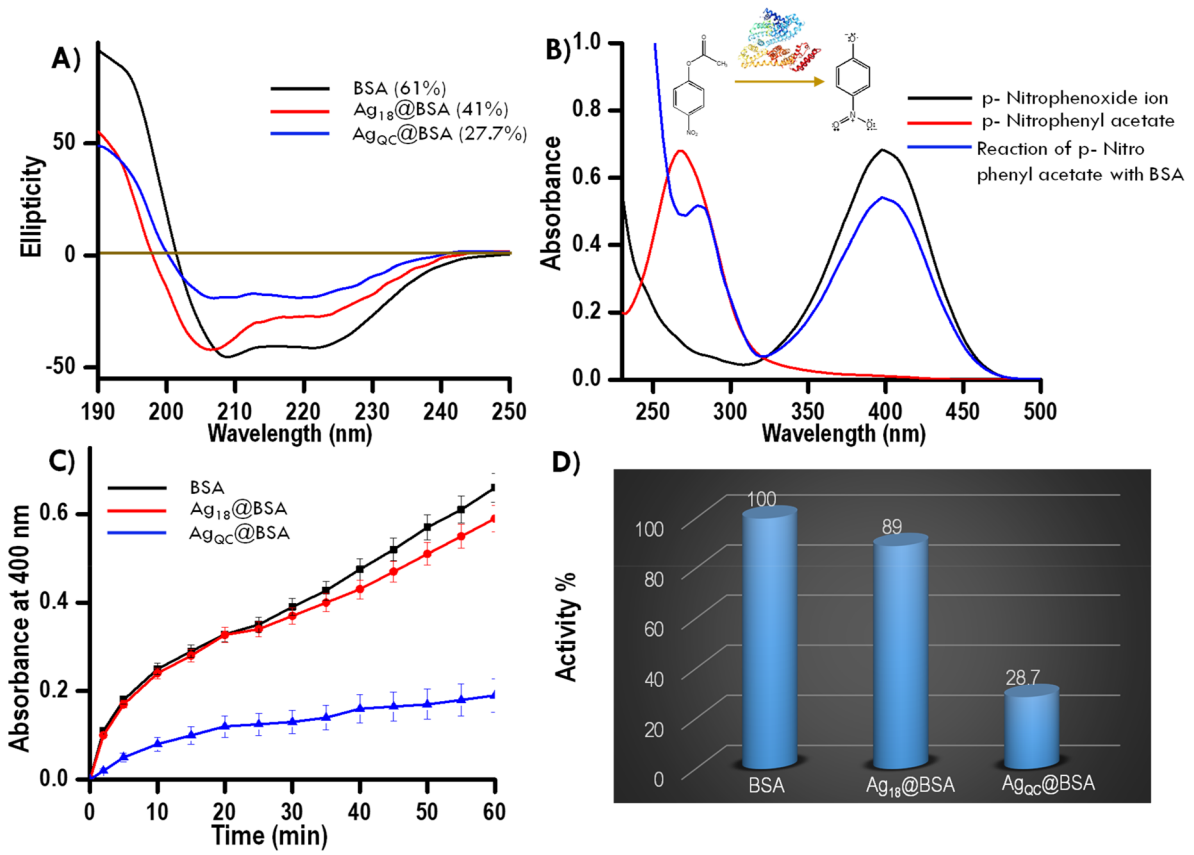

Figure 7. (A) CD spectra of the pure BSA an Ag_{18}@BSA and Ag_{QC}@BSA clusters. (B) UV−vis profile of esterase activity of BSA. (C) Ester hydrolysis reaction of pure protein and Ag_{18}@BSA and Ag_{QC}@BSA clusters as a function of time. (D) Percentage activity of pure protein and clusters.

reaction stops when the largest stable cluster that can be accommodated by these cysteine residues without significant alteration of the protein structure is formed, which turned out to be 18 for both BSA and HSA, probably due to their structural similarity. A schematic representation of this probable reaction mechanism is shown in Figure 5. Since preformed Ag(0) species are involved in the cluster formation, the process did not require the addition of a reducing agent. Formation of Ag_{18}@BSA cluster was not observed through the reaction of BSA with citrate-capped silver nanoparticles as well as with thiol (glutathione)-protected Ag clusters (Figure S9), presumably due to their enhanced stability, restricting them from producing the Ag(0) or Ag_n species needed in the process.

Cluster as Potential Bioimaging Probe. Entrapment of the metal core inside the biomolecular template through a formation of a strong M−S bond is expected to make the Ag_{18}@BSA clusters biocompatible. Their potential cytotoxicity was evaluated by incubating HeLa cells with the NCs and accessing the viability of these cells after 24 h through resazurin assay (results are shown in Figure S10). This confirmed the biocompatibility of the as-synthesized Ag_{18}@BSA NCs.

Their bright red luminescence can potentially be exploited for bioimaging applications given their ultrahigh stability in the biologically relevant conditions. Furthermore, the cluster being made at neutral pH eliminates the possibility of pH-induced changes in luminescence in physiological conditions. HeLa cells were used to study the cellular uptake without any special purification or conjugation of as-synthesized clusters. Attachment of the clusters along the cell membrane was observed after 5 h of incubation (Figure S11). The cluster gradually diffused into the cytosol and was observed to be completely internalized after 24 h (Figure 6). Three-dimensional reconstruction of the corresponding cells (Figure 6E and video V1) from the z stack images (shown in Figure S12) confirmed the localization of the clusters in the cytoplasm, demonstrating the cluster to be an excellent bioimaging probe. The cell nucleus was stained with DAPI in these experiments.

Retention of Protein Structure and Bioactivity. Reactions performed at solutions of high pH or use of strong reducing agents are thought to be the reasons for large changes in the secondary structure of the protein during cluster formation. Since the aforementioned process using a preformed cluster as precursor involves neither, retention of the protein structure to a greater degree is expected in the Ag_{18}@BSA. Conformational change in the protein structure can be measured by the change in the CD (circular dichroism) spectrum, which is shown in Figure 7A. The fraction of α-helix, a measure of the conformational change, was calculated for both Ag_{18}@BSA and Ag_{QC}@BSA clusters (synthesized through conventional route) from CD spectra. A higher degree of retention of α-helicity was indeed observed in Ag_{18}@BSA (41%) over Ag_{QC}@BSA (27.7%), confirming lesser alteration of the protein structure in the new synthetic methodology.

Function or bioactivity of a protein is also closely related to its structural integrity. BSA is known to possess esterase activity,[47,53−55] the ability to catalyze the hydrolysis of esters into component acids and alcohols. The retention of this

DOI: 10.1021/acs.jpcc.9b07765
J. Phys. Chem. C XXXX, XXX, XXX−XXX

biological function in Ag_{18}@BSA was tested using PNA as a model compound and was compared with that of Ag_{QC}@BSA. PNA shows a peak around 270 nm in its UV−vis spectrum (red trace, Figure 7B). This characteristic feature of PNA changes in the presence of BSA (blue trace, Figure 7B) to give a peak around 400 nm, indicating the formation of the phenolate ion (black trace, Figure 7B) in the solution through hydrolysis. Kinetics of the catalyzed hydrolysis of PNA was monitored by following the concentration of the phenolate ions through UV−vis spectroscopy (Figure 7c). After 1 h of reaction, Ag_{18}@BSA was found to be 89% as active as parent BSA, compared to only 28.7% in the case of Ag_{QC}@BSA (Figure 7D). This can be related to the changes in the primary and secondary structures of the protein during the synthesis of Ag_{QC}@BSA. Basic medium used in this conventional protocol can modify the tyrosine and arginine residues, thought to be responsible for the esterase activity of BSA,[56,57] causing disruption of H bonds and electrostatic interactions, leading to the loss in helicity. On the other hand, synthesis of Ag_{18}@BSA involves only the capture and encapsulation of Ag clusters from solution and retains the structural integrity as well the bioactivity of the protein. This improved bioactivity is supported by studies using Ag_{13}@Lf as well. Lf possesses several enzymatic activities; among them, phosphatase activity was monitored in a similar way for native Lf and the Ag_{13}@Lf. The cluster showed 90% catalytic activity (Figure S13).

CONCLUSIONS

We introduced a new protocol to synthesize red luminescent protein-protected clusters using preformed clusters as the metal source. Internalization of the silver clusters released in solution from nonluminescent phosphine-protected precursor cluster by the protein was manifested in the change of the luminescence of the solution. The presence of an 18 Ag atom core associated with each protein molecule in the final cluster was identified through MALDI MS, and the mechanism of formation was elucidated from time-dependent mass spectra. A higher degree of structural intactness of the protein in the formed cluster could be achieved by this protocol. This resulted in the addition of extra functionality to the proteins while the inherent bioactivity is retained, addressing a major problem associated with the conventional method of synthesis. The clusters were found to be excellent luminescent probes for cancer cell imaging. The combination of stable yet sensitive luminescence of the clusters formed inside minimal structurally altered and functionally active proteins is expected to aid in the further development of biomedical applications of such clusters.

ASSOCIATED CONTENT

Supporting Information

The Supporting Information is available free of charge at https://pubs.acs.org/doi/10.1021/acs.jpcc.9b07765.

Protocols for the synthesis of [Ag_{18}HSA] and [Ag_{13}Lf], EDS spectrum of the precipitate, SEM EDS and XPS of the Ag_{18}@BSA, characterization of Ag_{18}@HSA and Ag_{13}@Lf, time-dependent luminescence profile of Ag_{18}@BSA and reaction of $[Ag_{18}H_{16}(TPP)_{10}]^{2+}$ with Ag nanoparticles, cell viability test, confocal fluorescence image of NCs incubated HeLa cells (PDF)

Three-dimensional reconstruction of the corresponding cells (AVI)

AUTHOR INFORMATION

Corresponding Author

*E-mail: pradeep@iitm.ac.in.

ORCID

Anirban Som: 0000-0002-6646-679X

Thalappil Pradeep: 0000-0003-3174-534X

Notes

The authors declare no competing financial interest.

ACKNOWLEDGMENTS

We thank the Department of Science and Technology, Government of India, for continuous support of our research program on nanomaterials. D.G. thanks IIT Madras for student fellowships.

REFERENCES

(1) Xie, J.; Zheng, Y.; Ying, J. Y. Protein-Directed Synthesis of Highly Fluorescent Gold Nanoclusters. *J. Am. Chem. Soc.* **2009**, *131*, 888−889.

(2) Xavier, P. L.; Chaudhari, K.; Baksi, A.; Pradeep, T. Protein-Protected Luminescent Noble Metal Quantum Clusters: An Emerging Trend in Atomic Cluster Nanoscience. *Nano Rev.* **2012**, *3*, 14767.

(3) Chevrier, D. M.; Thanthirige, V. D.; Luo, Z.; Driscoll, S.; Cho, P.; MacDonald, M. A.; Yao, Q.; Guda, R.; Xie, J.; Johnson, E. R.; Chatt, A.; Zheng, N.; Zhang, P. Structure and Formation of Highly Luminescent Protein-Stabilized Gold Clusters. *Chem. Sci.* **2018**, *9*, 2782−2790.

(4) Chakraborty, I.; Pradeep, T. Atomically Precise Clusters of Noble Metals: Emerging Link between Atoms and Nanoparticles. *Chem. Rev. (Washington, DC, U. S.)* **2017**, *117*, 8208−8271.

(5) Diez, I.; Ras, R. H. A. Fluorescent Silver Nanoclusters. *Nanoscale* **2011**, *3*, 1963−1970.

(6) Goswami, N.; Zheng, K.; Xie, J. Bio-Ncs - the Marriage of Ultrasmall Metal Nanoclusters with Biomolecules. *Nanoscale* **2014**, *6*, 13328−13347.

(7) Sun, C.; Yang, H.; Yuan, Y.; Tian, X.; Wang, L.; Guo, Y.; Xu, L.; Lei, J.; Gao, N.; Anderson, G. J.; Liang, X.-J.; Chen, C.; Zhao, Y.; Nie, G. Controlling Assembly of Paired Gold Clusters within Apoferritin Nanoreactor for in Vivo Kidney Targeting and Biomedical Imaging. *J. Am. Chem. Soc.* **2011**, *133*, 8617−8624.

(8) Mathew, A.; Sajanlal, P. R.; Pradeep, T. Selective Visual Detection of TNT at the Sub-Zeptomole Level. *Angew. Chem., Int. Ed.* **2012**, *51*, 9596−9600.

(9) Hu, D.; Sheng, Z.; Gong, P.; Zhang, P.; Cai, L. Highly Selective Fluorescent Sensors for Hg^{2+} Based on Bovine Serum Albumin-Capped Gold Nanoclusters. *Analyst (Cambridge, U. K.)* **2010**, *135*, 1411−1416.

(10) Chen, T.-H.; Tseng, W.-L. (Lysozyme Type Vi)-Stabilized Au_8 Clusters: Synthesis Mechanism and Application for Sensing of Glutathione in a Single Drop of Blood. *Small* **2012**, *8*, 1912−1919.

(11) Song, X.-R.; Goswami, N.; Yang, H.-H.; Xie, J. Functionalization of Metal Nanoclusters for Biomedical Applications. *Analyst (Cambridge, U. K.)* **2016**, *141*, 3126−3140.

(12) Wang, Y.; Chen, J.-T.; Yan, X.-P. Fabrication of Transferrin Functionalized Gold Nanoclusters/Graphene Oxide Nanocomposite for Turn-on near-Infrared Fluorescent Bioimaging of Cancer Cells and Small Animals. *Anal. Chem. (Washington, DC, U. S.)* **2013**, *85*, 2529−2535.

(13) Mathew, M. S.; Davis, J.; Joseph, K. Green Synthesis of a Plant-Derived Protein Protected Copper Quantum Cluster for Intrauterine Device Application. *Analyst (Cambridge, U. K.)* **2018**, *143*, 3841−3849.

(14) Basu, K.; Gayen, K.; Mitra, T.; Baral, A.; Roy, S. S.; Banerjee, A. Different Color Emissive Copper Nanoclusters for Cancer Cell Imaging. *ChemNanoMat* **2017**, *3*, 808−814.

DOI: 10.1021/acs.jpcc.9b07765
J. Phys. Chem. C XXXX, XXX, XXX−XXX

(15) Wang, Y.; Chen, J.; Irudayaraj, J. Nuclear Targeting Dynamics of Gold Nanoclusters for Enhanced Therapy of Her2+ Breast Cancer. *ACS Nano* **2011**, *5*, 9718−9725.
(16) Yu, Y.; New, S. Y.; Xie, J.; Su, X.; Tan, Y. N. Protein-Based Fluorescent Metal Nanoclusters for Small Molecular Drug Screening. *Chem. Commun. (Cambridge, U. K.)* **2014**, *50*, 13805−13808.
(17) Zhang, A.; Tu, Y.; Qin, S.; Li, Y.; Zhou, J.; Chen, N.; Lu, Q.; Zhang, B. Gold Nanoclusters as Contrast Agents for Fluorescent and X-Ray Dual-Modality Imaging. *J. Colloid Interface Sci.* **2012**, *372*, 239−244.
(18) Zhou, W.; Cao, Y.; Sui, D.; Guan, W.; Lu, C.; Xie, J. Ultrastable BSA-Capped Gold Nanoclusters with a Polymer-Like Shielding Layer against Reactive Oxygen Species in Living Cells. *Nanoscale* **2016**, *8*, 9614−9620.
(19) Wu, X.; He, X.; Wang, K.; Xie, C.; Zhou, B.; Qing, Z. Ultrasmall near-Infrared Gold Nanoclusters for Tumor Fluorescence Imaging in Vivo. *Nanoscale* **2010**, *2*, 2244−2249.
(20) Zhang, X.-D.; Chen, J.; Luo, Z.; Wu, D.; Shen, X.; Song, S.-S.; Sun, Y.-M.; Liu, P.-X.; Zhao, J.; Huo, S.; Fan, S.; Fan, F.; Liang, X.-J.; Xie, J. Enhanced Tumor Accumulation of Sub-2 Nm Gold Nanoclusters for Cancer Radiation Therapy. *Adv. Healthcare Mater.* **2014**, *3*, 133−141.
(21) Habeeb Muhammed, M. A.; Verma, P. K.; Pal, S. K.; Retnakumari, A.; Koyakutty, M.; Nair, S.; Pradeep, T. Luminescent Quantum Clusters of Gold in Bulk by Albumin-Induced Core Etching of Nanoparticles: Metal Ion Sensing, Metal-Enhanced Luminescence, and Biolabeling. *Chem. - Eur. J.* **2010**, *16*, 10103−10112.
(22) Lin, C.-A. J.; Yang, T.-Y.; Lee, C.-H.; Huang, S. H.; Sperling, R. A.; Zanella, M.; Li, J. K.; Shen, J.-L.; Wang, H.-H.; Yeh, H.-I.; Parak, W. J.; Chang, W. H. Synthesis, Characterization, and Bioconjugation of Fluorescent Gold Nanoclusters toward Biological Labeling Applications. *ACS Nano* **2009**, *3*, 395−401.
(23) Fernandez-Iglesias, N.; Bettmer, J. Synthesis, Purification and Mass Spectrometric Characterisation of a Fluorescent Au_9@BSA Nanocluster and Its Enzymatic Digestion by Trypsin. *Nanoscale* **2014**, *6*, 716−721.
(24) Yue, Y.; Liu, T.-Y.; Li, H.-W.; Liu, Z.; Wu, Y. Microwave-Assisted Synthesis of Bsa-Protected Small Gold Nanoclusters and Their Fluorescence-Enhanced Sensing of Silver(I) Ions. *Nanoscale* **2012**, *4*, 2251−2254.
(25) Mohanty, J. S.; Baksi, A.; Lee, H.; Pradeep, T. Noble Metal Clusters Protected with Mixed Proteins Exhibit Intense Photoluminescence. *RSC Adv.* **2015**, *5*, 48039−48045.
(26) Le Guevel, X.; Hotzer, B.; Jung, G.; Hollemeyer, K.; Trouillet, V.; Schneider, M. Formation of Fluorescent Metal (Au, Ag) Nanoclusters Capped in Bovine Serum Albumin Followed by Fluorescence and Spectroscopy. *J. Phys. Chem. C* **2011**, *115*, 10955−10963.
(27) Mathew, A.; Sajanlal, P. R.; Pradeep, T. A Fifteen Atom Silver Cluster Confined in Bovine Serum Albumin. *J. Mater. Chem.* **2011**, *21*, 11205−11212.
(28) Mohanty, J. S.; Xavier, P. L.; Chaudhari, K.; Bootharaju, M. S.; Goswami, N.; Pal, S. K.; Pradeep, T. Luminescent, Bimetallic AuAg Alloy Quantum Clusters in Protein Templates. *Nanoscale* **2012**, *4*, 4255−4262.
(29) Chan, P.-H.; Chen, Y.-C. Human Serum Albumin Stabilized Gold Nanoclusters as Selective Luminescent Probes for Staphylococcus Aureus and Methicillin-Resistant Staphylococcus Aureus. *Anal. Chem. (Washington, DC, U. S.)* **2012**, *84*, 8952−8956.
(30) Xavier, P. L.; Chaudhari, K.; Verma, P. K.; Pal, S. K.; Pradeep, T. Luminescent Quantum Clusters of Gold in Transferrin Family Protein, Lactoferrin Exhibiting Fret. *Nanoscale* **2010**, *2*, 2769−2776.
(31) Chaudhari, K.; Xavier, P. L.; Pradeep, T. Understanding the Evolution of Luminescent Gold Quantum Clusters in Protein Templates. *ACS Nano* **2011**, *5*, 8816−8827.
(32) Le Guevel, X.; Daum, N.; Schneider, M. Synthesis and Characterization of Human Transferrin-Stabilized Gold Nanoclusters. *Nanotechnology* **2011**, *22*, 275103.
(33) Kawasaki, H.; Hamaguchi, K.; Osaka, I.; Arakawa, R. pH-Dependent Synthesis of Pepsin-Mediated Gold Nanoclusters with Blue-, Green-, and Red-Fluorescent Emission. *Adv. Funct. Mater.* **2011**, *21*, 3508−3515.
(34) Wen, F.; Dong, Y.; Feng, L.; Wang, S.; Zhang, S.; Zhang, X. Horseradish Peroxidase Functionalized Fluorescent Gold Nanoclusters for Hydrogen Peroxide Sensing. *Anal. Chem. (Washington, DC, U. S.)* **2011**, *83*, 1193−1196.
(35) Li, M.; Yang, D.-P.; Wang, X.; Lu, J.; Cui, D. Mixed Protein-Templated Luminescent Metal Clusters (Au and Pt) for H_2O_2 Sensing. *Nanoscale Res. Lett.* **2013**, *8*, 182.
(36) Shi, H.; Ou, M. Y.; Cao, J. P.; Chen, G. F. Synthesis of Ovalbumin-Stabilized Highly Fluorescent Gold Nanoclusters and Their Application as an Hg^{2+} Sensor. *RSC Adv.* **2015**, *5*, 86740−86745.
(37) Liu, C.-L.; Wu, H.-T.; Hsiao, Y.-H.; Lai, C.-W.; Shih, C.-W.; Peng, Y.-K.; Tang, K.-C.; Chang, H.-W.; Chien, Y.-C.; Hsiao, J.-K.; Cheng, J.-T.; Chou, P.-T. Insulin-Directed Synthesis of Fluorescent Gold Nanoclusters: Preservation of Insulin Bioactivity and Versatility in Cell Imaging. *Angew. Chem., Int. Ed.* **2011**, *50*, 7056−7060.
(38) Baksi, A.; Xavier, P. L.; Chaudhari, K.; Goswami, N.; Pal, S. K.; Pradeep, T. Protein-Encapsulated Gold Cluster Aggregates: The Case of Lysozyme. *Nanoscale* **2013**, *5*, 2009−2016.
(39) Kawasaki, H.; Yoshimura, K.; Hamaguchi, K.; Arakawa, R. Trypsin-Stabilized Fluorescent Gold Nanocluster for Sensitive and Selective Hg^{2+} Detection. *Anal. Sci.* **2011**, *27*, 591−596.
(40) Yu, Y.; Luo, Z.; Teo, C. S.; Tan, Y. N.; Xie, J. Tailoring the Protein Conformation to Synthesize Different-Sized Gold Nanoclusters. *Chem. Commun. (Cambridge, U. K.)* **2013**, *49*, 9740−9742.
(41) Gao, X.; Chan, W. C. W.; Nie, S. Quantum-Dot Nanocrystals for Ultrasensitive Biological Labeling and Multicolor Optical Encoding. *J. Biomed. Opt.* **2002**, *7*, 532−537.
(42) Russell, B. A.; Jachimska, B.; Komorek, P.; Mulheran, P. A.; Chen, Y. Lysozyme Encapsulated Gold Nanoclusters: Effects of Cluster Synthesis on Natural Protein Characteristics. *Phys. Chem. Chem. Phys.* **2017**, *19*, 7228−7235.
(43) Soleilhac, A.; Bertorelle, F.; Antoine, R. Sizing Protein-Templated Gold Nanoclusters by Time Resolved Fluorescence Anisotropy Decay Measurements. *Spectrochim. Acta, Part A* **2018**, *193*, 283−288.
(44) Jin, R.; Zeng, C.; Zhou, M.; Chen, Y. Atomically Precise Colloidal Metal Nanoclusters and Nanoparticles: Fundamentals and Opportunities. *Chem. Rev. (Washington, DC, U. S.)* **2016**, *116*, 10346−10413.
(45) Bootharaju, M. S.; Dey, R.; Gevers, L. E.; Hedhili, M. N.; Basset, J.-M.; Bakr, O. M. A New Class of Atomically Precise, Hydride-Rich Silver Nanoclusters Co-Protected by Phosphines. *J. Am. Chem. Soc.* **2016**, *138*, 13770−13773.
(46) Ghosh, A.; Bodiuzzaman, M.; Nag, A.; Jash, M.; Baksi, A.; Pradeep, T. Sequential Dihydrogen Desorption from Hydride-Protected Atomically Precise Silver Clusters and the Formation of Naked Clusters in the Gas Phase. *ACS Nano* **2017**, *11*, 11145−11151.
(47) De, P.; Li, M.; Gondi, S. R.; Sumerlin, B. S. Temperature-Regulated Activity of Responsive Polymer-Protein Conjugates Prepared by Grafting-from Via Raft Polymerization. *J. Am. Chem. Soc.* **2008**, *130*, 11288−11289.
(48) Goswami, N.; Giri, A.; Bootharaju, M. S.; Xavier, P. L.; Pradeep, T.; Pal, S. K. Copper Quantum Clusters in Protein Matrix: Potential Sensor of Pb^{2+} Ion. *Anal. Chem. (Washington, DC, U. S.)* **2011**, *83*, 9676−9680.
(49) Chan, R.; Chen, V.; Bucknall, M. P. Quantitative Analysis of Membrane Fouling by Protein Mixtures Using MALDI-MS. *Biotechnol. Bioeng.* **2004**, *85*, 190−201.
(50) Ghosh, D.; Baksi, A.; Mudedla, S. K.; Nag, A.; Ganayee, M. A.; Subramanian, V.; Pradeep, T. Gold-Induced Unfolding of Lysozyme: Toward the Formation of Luminescent Clusters. *J. Phys. Chem. C* **2017**, *121*, 13335−13344.
(51) Ghosh, D.; Mudedla, S. K.; Islam, M. R.; Subramanian, V.; Pradeep, T. Conformational Changes of Protein Upon Encapsulation

DOI: 10.1021/acs.jpcc.9b07765
J. Phys. Chem. C XXXX, XXX, XXX−XXX

of Noble Metal Clusters: An Investigation by Hydrogen/Deuterium Exchange Mass Spectrometry. *J. Phys. Chem. C* **2019**, *123*, 17598−17605.
(52) Maity, B.; Abe, S.; Ueno, T. Observation of Gold Sub-Nanocluster Nucleation within a Crystalline Protein Cage. *Nat. Commun.* **2017**, *8*, 14820.
(53) Chakraborty, S.; Joshi, P.; Shanker, V.; Ansari, Z. A.; Singh, S. P.; Chakrabarti, P. Contrasting Effect of Gold Nanoparticles and Nanorods with Different Surface Modifications on the Structure and Activity of Bovine Serum Albumin. *Langmuir* **2011**, *27*, 7722−7731.
(54) Cordova, J.; Ryan, J. D.; Boonyaratanakornkit, B. B.; Clark, D. S. Esterase Activity of Bovine Serum Albumin up to 160°C: A New Benchmark for Biocatalysis. *Enzyme Microb. Technol.* **2008**, *42*, 278−283.
(55) Sakurai, Y.; Ma, S.-F.; Watanabe, H.; Yamaotsu, N.; Hirono, S.; Kurono, Y.; Kragh-Hansen, U.; Otagiri, M. Esterase-Like Activity of Serum Albumin: Characterization of Its Structural Chemistry Using P-Nitrophenyl Esters as Substrates. *Pharm. Res.* **2004**, *21*, 285−292.
(56) Ahmad, B.; Kamal, M. Z.; Khan, R. H. Alkali-Induced Conformational Transition in Different Domains of Bovine Serum Albumin. *Protein Pept. Lett.* **2004**, *11*, 307−315.
(57) t Hart, B. J.; Wilting, J.; de Gier, J. J. Evidence for Distinct Consecutive Steps in the Neutral to Base Transition of Human Serum Albumin. *Biochem. Pharmacol.* **1986**, *35*, 1005−1009.

DOI: 10.1021/acs.jpcc.9b07765
J. Phys. Chem. C XXXX, XXX, XXX−XXX